Supplymentary Information for "Mapping the influence of impurity interaction energy on nucleation in a lattice-gas model of solute precipitation"

Authors: Dipanjan Mandal and David Quigley
Affiliation: Department of Physics, University of Warwick, Coventry CV4 7AL, United Kingdom

In this supplementary information we provide additional data required to support the findings of the paper.

0.1 *Saturation of the free energy barrier and the nucleation rate:*

As discussed in Section 4 of the paper, when impurities are dynamic and interaction energy is anti-symmetric ($\varepsilon_+ = -\varepsilon_- = \varepsilon$), the nucleation free energy barrier height and the nucleation rate do not depend on the interaction strength after a certain threshold value of the repulsive interaction energy ε_+, beyond this limit all impurities are removed from the cluster due to strong repulsive interaction with solute. We observe such saturation in free energy barrier with respect to the anti-symmetric interaction energy at both low $\rho_i = 0.004$ and high $\rho_i = 0.02$ impurity density (see Fig. S1). Another example, for intermediate impurity density $\rho_i = 0.008$, is shown in Fig. S2 with parameter values $\beta J = 0.67$, $\beta \Delta \mu = 0.067$ and $\alpha = 0.05$.
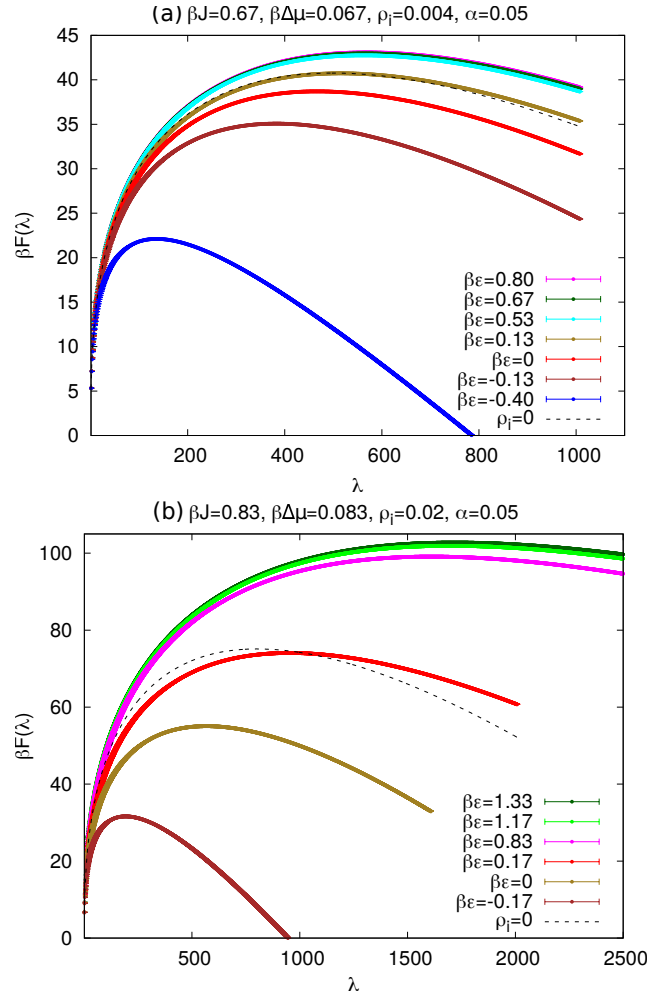

Figure S1 Nucleation free energy with dynamic impurities, varying anti-symmetric interaction energy $\beta \varepsilon_+ = -\beta \varepsilon_- = \beta \varepsilon$, for (a) $\beta J = 0.67$, $\beta \Delta \mu = 0.067$, $\rho_i = 0.004$ and (b) $\beta J = 0.83$, $\beta \Delta \mu = 0.083$, $\rho_i = 0.02$ with fixed mobility parameter $\alpha = 0.05$. Free energy barrier for the system without impurities ($\rho_i = 0$) is plotted by black dotted line for comparison. The saturation in barrier height is seen for both low and high impurity density unlike the static impurities as shown in Fig. S3.

In the case of static impurities, we do not see such saturation in free energy barrier and nucleation rate above a certain impurity density threshold as discussed in Section 3 of the paper. For a random impurity configuration, the saturation criterion could be related with competition between the size of the largest void area without impurities and the critical cluster size. If the size of the largest void area is greater than the critical cluster size, we expect to see the saturation in the free energy barrier even for static impurities. Examining the detailed statistics of void site and distribution expected from a uniform distribution of impurities could in principle lead to an estimate of that threshold.

For the impurity density $\rho_i = 0.004$, we observe saturation both in free energy barrier [see Fig. S3(a)] and nucleation rate [see Fig. S4]
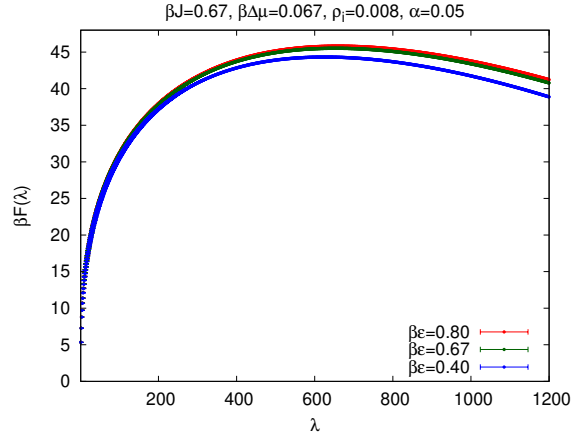
Figure S2 Saturation of nucleation free energy barrier for anti-symmetric interaction energy $\beta\varepsilon_+ = -\beta\varepsilon_- = \beta\varepsilon$ with fixed $\beta J = 0.67$, $\beta\Delta\mu = 0.067$ in the presence of dynamic impurities of density $\rho_i = 0.008$ with $\alpha = 0.05$.
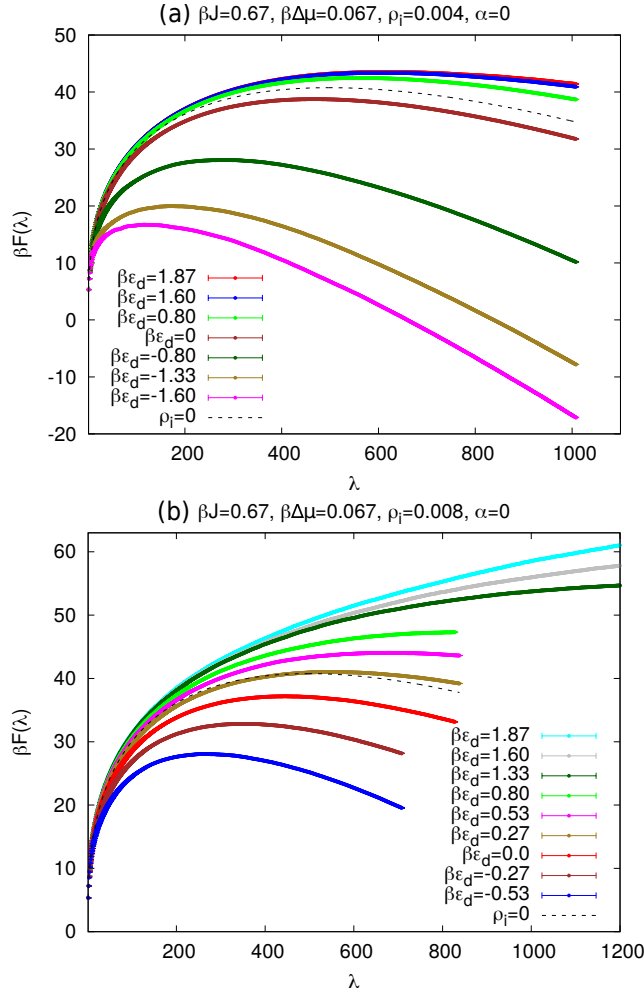

Figure S3 Nucleation free energy with varying dimensionless interaction energy difference $\beta\varepsilon_d$ with fixed $\beta J = 0.67$, $\beta\Delta\mu = 0.067$ for system size $L = 100$ at static impurity density (a) $\rho_i = 0.004$ and (b) $\rho_i = 0.008$. We see no further increase in free energy barrier height with increasing $\beta\varepsilon_d$ when $\rho_i = 0.004$ or lower, i.e., when the impurities are sparsely distributed so that a critical cluster can fit in the void space without interacting with impurities. This behaviour in barrier height is not observed for $\rho_i = 0.008$ when impurity density is higher. Free energy barrier for the system without impurities ($\rho_i = 0$) is plotted by dotted line for comparison.

with increasing $\beta\varepsilon_d$. However, at higher impurity density $\rho_i = 0.008$, when the average void area excluding impurities decreases, we observe a monotonic increase in barrier height without saturation as $\beta\varepsilon_d$ is increased [see Fig. S3(b)]. We also note the differences in
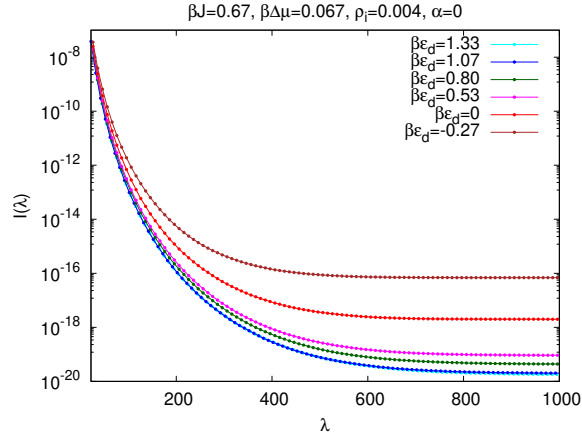
Figure S4 Rate of obtaining a cluster of size λ starting from a metastable solution phase for different interaction energy difference $\beta\varepsilon_d$ at fixed $\beta J = 0.67$, $\beta\Delta\mu = 0.067$ and $\rho_i = 0.004$ with static impurities. The constant value of $I(\lambda)$ for large λ is the nucleation rate.

shape of saturated free energy between static and dynamic cases at $\rho_i = 0.004$. Unlike dynamic impurities, the free energy curve becomes flatter in the case of static impurities and starts to deviate from the standard form of the free energy function assumed in classical nucleation theory as given in Eq.4 (see $\beta\varepsilon_d = 1.6$ curve in Fig.S7 and high positive $\beta\varepsilon_d$ curves in Fig. S3). The confinement/constraint imposed by the immobile impurities could be responsible for this behaviour as it forces nuclei into shape with surface area to perimeter ratios that differ from the ideal case.

0.2 *Free energy barrier with symmetric interaction energy ($\varepsilon_+ = \varepsilon_- = \varepsilon$):*
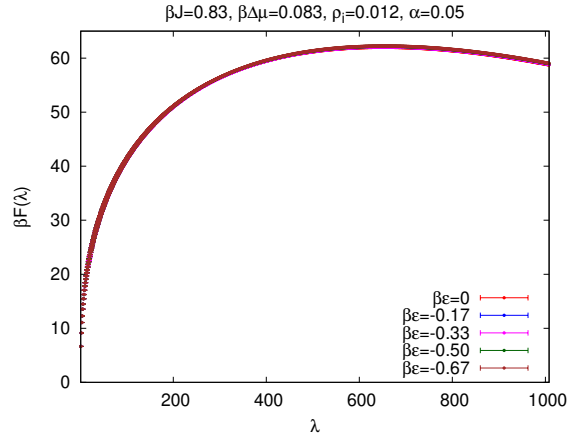

Figure S5 Nucleation free energy with dynamic impurities, varying symmetric interaction strengths $\beta\varepsilon_+ = \beta\varepsilon_- = \beta\varepsilon$ for $\beta J = 0.83$, $\beta\Delta\mu = 0.083$, $\rho_i = 0.012$ and $\alpha = 0.05$. The plotted range of interaction energy lie in *surfactant* regime of the behaviour map. We do not see any variation in barrier height.

In the *surfactant* regime of the behaviour map we do not see much variation in the nucleation rate as shown in Fig. 8(a) of the paper, for dynamic impurities with $\beta J = 0.83$, $\beta\Delta\mu = 0.083$, $\rho_i = 0.012$ and $\alpha = 0.05$. Similar behaviour is reflected in free energy plots for different values of symmetric interaction energies that belong to the *surfactant* regime as shown in Fig. S5.

0.3 *Decrement in free energy barrier height due to mobile impurities:*

As observed in Section 4, the free energy barrier height to nucleation decreases when impurities are dynamic compared to the static case for same set of interaction energies as shown in Fig. S6 (see Fig. 2(a) of the paper). In this case the interaction energies are anti-symmetric ($\beta\varepsilon_+ = -\beta\varepsilon_- = 0.4$) and other parameter values are $\beta J = 0.67$, $\beta\Delta\mu = 0.067$ and $\rho_i = 0.008$. Dynamic impurities enhance the nucleation rate by decreasing the barrier height. In this example the microscopic interaction between impurity-solute and impurity-solvent are respectively weakly-repulsive and weakly-attractive and lies at the boundary of the *surfactant* regime of the behaviour map. We also observed similar decrement in barrier height in our earlier work [D. Mandal and D. Quigley, Soft Matter, 2021, 17, 8642–8650] for impurities with neutral interactions. However, in that case, because of the neutral interaction impurities prefer to stay at the boundaries of the cluster, it reduces the interfacial free energy.
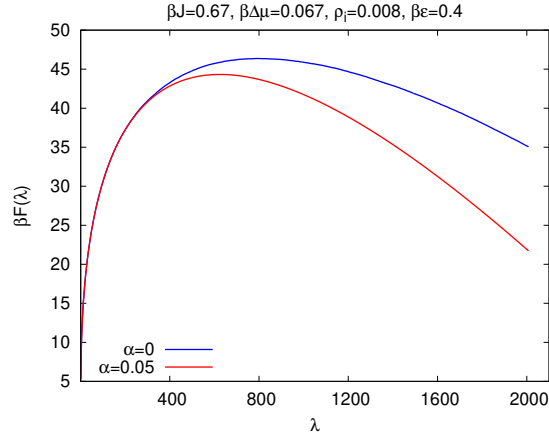
Figure S6 Comparison of the free energy barrier for static ($\alpha = 0$) and dynamic ($\alpha = 0.05$) impurities with same anti-symmetric interaction energy $\beta\varepsilon_+ = -\beta\varepsilon_- = 0.4$ for $\beta J = 0.67$ with $\rho_i = 0.008$.

0.4 *Fitting free energy barrier:*

Fitting of free energy to the expression given in Eq. 4 in the case of static impurities with density $\rho_i = 0.004$, $\beta J = 0.67$ and $\beta\Delta\mu = 0.067$ for different $\beta\varepsilon_d$ is shown in Fig. S7, where we allow the surface A_s and bulk A_b terms to vary from the $\rho_i = 0$ case. We see that A_s increases and A_b decreases monotonically with increasing $\beta\varepsilon_d$ from negative to positive values. The fitting becomes more accurate with decreasing $\beta\varepsilon_d$.
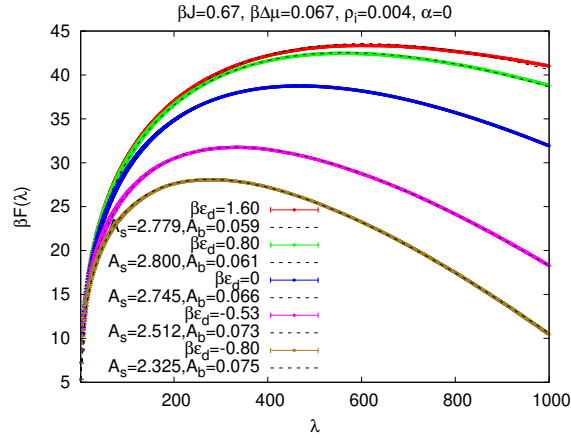

Figure S7 Fitting of the free energy expression given in Eq. 4 with the free energy obtained from umbrella sampling method varying $\beta\varepsilon_d$ for static impurities with $\beta J = 0.67$, $\beta\Delta\mu = 0.067$ and $\rho_i = 0.004$.

Similar fitting of calculated free energy with Eq. 4 for dynamic impurities with $\beta J = 0.67$, $\beta\Delta\mu = 0.067$, $\rho_i = 0.004$ and $\alpha = 0.05$ is shown in Fig. S8 for different $\beta\varepsilon$. We see monotonic decrease and monotonic increase of the bulk and surface terms respectively with increasing $\beta\varepsilon$ until they converge to non-zero finite values after entering into the inert-spectator regime of the behaviour map. We note that, for pure Ising model at low temperatures $\Delta g \approx \Delta\mu$, and from Fig. S8 we see that this relation holds for neutral impurities, as $A_b \approx \beta\Delta\mu$ when $\beta\varepsilon = 0$, but not for non-zero interaction energies.

0.5 *Nucleation rate and diffusion coefficient D_c:*

The Becker-Doring-Zeldovitch nucleation rate I_{BDZ} is calculated using Eq. 5 of the paper for high $\rho_i = 0.02$ and intermediate $\rho_i = 0.012$ impurity densities. For that, the diffusion coefficient D_c is calculated after performing independent simulations starting from the critical cluster size at time $t = 0$ and calculating the slope of the mean squared deviation of cluster size with time t. Estimated values of D_c corresponding to plots displayed in Fig. S9 are written in column 4 of Table S1. The values of different parameters required for calculating I_{BDZ} is given in Table S1 and Table S2 for $\rho_i = 0.02$ (anti-symmetric interaction energy) and $\rho_i = 0.012$ (symmetric interaction energy) respectively. In the final column the nucleation rate obtained from independent forward flux sampling simulations I_{FFS} is written. The results for I_{BDZ} and I_{FFS} match quite well for the range of interaction energies considered in both tables.
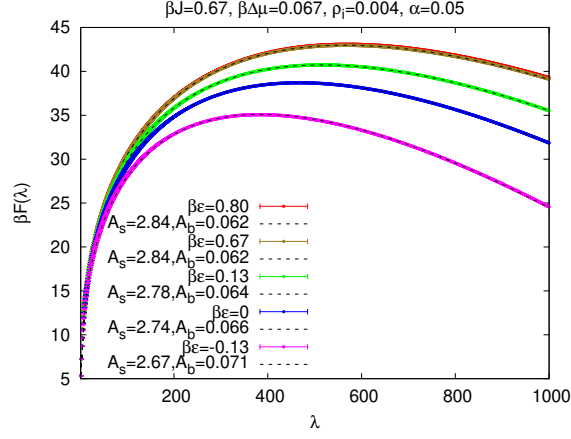
Figure S8 Fitting of the free energy expression given in Eq. 4 with the free energy obtained from umbrella sampling method for dynamic impurities and varying anti-symmetric interaction energy $\beta\varepsilon_+ = -\beta\varepsilon_- = \beta\varepsilon$ with $\beta J = 0.67$, $\beta\Delta\mu = 0.067$, $\rho_i = 0.004$ and $\alpha = 0.05$.
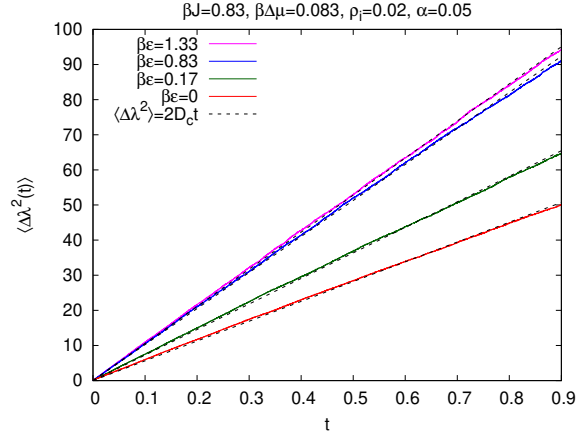

Figure S9 Linear fitting of diffusivity $\langle\Delta\lambda^2\rangle = 2D_c t$ obtained from simulation for dynamic impurities with $\beta J = 0.83$, $\beta\Delta\mu = 0.083$, $\rho_i = 0.02$ and $\alpha = 0.05$. Initial size of the cluster is set to the critical cluster size calculated from the position of the maxima in the respective $F(\lambda)$ vs. λ plots.

$\beta\varepsilon$	λ_c	$\beta F(\lambda_c)$	D_c	I_{BDZ}	I_{FFS}
1.33	1689	103.58	52.8	9×10^{-47}	1.7×10^{-46}
0.83	1584	99.26	51.3	6.8×10^{-45}	5.3×10^{-45}
0.17	942	73.69	36.4	8.8×10^{-34}	5.6×10^{-34}
0	571	55.21	28.2	1×10^{-25}	1.1×10^{-25}

Table S1 Comparison of nucleation rates obtained from Becker-Doring-Zeldovich analysis (I_{BD}) and forward flux sampling method (I_{FFS}) for $\beta J = 0.83$, $\rho_i = 0.02$ and $\alpha = 0.05$ with anti-symmetric interaction energy $\beta\varepsilon_+ = -\beta\varepsilon_- = \varepsilon$. The maximum error in determining I_{BDZ} and I_{FFS} are 80% and 10% respectively. The parameter values $\beta\varepsilon = 0$ and $\beta\varepsilon = 1.33$ lie in the surfactant and bulk-stabilizer regimes respectively.

$\beta\varepsilon$	λ_c	$\beta F(\lambda_c)$	D_c	I_{BDZ}	I_{FFS}
0.67	642	60.88	30.4	3.5×10^{-28}	7.8×10^{-28}
1.0	670	56.93	30.6	1.8×10^{-26}	2.5×10^{-26}
1.33	766	61.58	33.5	1.6×10^{-28}	6.7×10^{-28}

Table S2 Comparison of nucleation rates obtained from Becker-Doring-Zeldovich analysis (I_{BDZ}) and forward flux sampling method (I_{FFS}) for $\beta J = 0.83$, $\beta\Delta\mu = 0.083$, $\rho_i = 0.012$ and $\alpha = 0.05$ with symmetric interaction energy $\beta\varepsilon_+ = \beta\varepsilon_- = \varepsilon$. This range of $\beta\varepsilon$ belongs to the regime in which impurities act like heterogeneous nucleating sites.